Fluorescence microspectroscopy as a tool to study mechanism of nanoparticles delivery into living cancer cells

Zoran Arsov,[1,2] Iztok Urbančič,[1] Maja Garvas,[1] Daniele Biglino,[1,2] Ajasja Ljubetič,[1] Tilen Koklič,[1,2] and Janez Štrancar[1,2,*]

[1]*Laboratory of Biophysics, Department of Solid State Physics, Jožef Stefan Institute, Jamova 39, 1000 Ljubljana, Slovenia*

[2]*Center of Excellence NAMASTE, Jamova 39, 1000 Ljubljana, Slovenia*

**janez.strancar@ijs.si*

Abstract: Lack of better understanding of nanoparticles targeted delivery into cancer cells calls for advanced optical microscopy methodologies. Here we present a development of fluorescence microspectroscopy (spectral imaging) based on a white light spinning disk confocal microscope with emission wavelength selection by a liquid crystal tunable filter. Spectral contrasting of images was used to localize polymer nanoparticles and cell membranes labeled with fluorophores that have substantially overlapping spectra. In addition, fluorescence microspectroscopy enabled spatially-resolved detection of small but significant effects of local molecular environment on the properties of environment-sensitive fluorescent probe. The observed spectral shift suggests that the delivery of suitably composed cancerostatic alkylphospholipid nanoparticles into living cancer cells might rely on the fusion with plasma cell membrane.

OCIS codes: (170.0170) Medical optics and biotechnology; (170.2520) Fluorescence microscopy; (110.4234) Multispectral and hyperspectral imaging; (300.6280) Spectroscopy, fluorescence and luminescence; (230.7408) Wavelength filtering devices

References and links

1. K. Loomis, K. McNeeley, and R. V. Bellamkonda, "Nanoparticles with targeting, triggered release, and imaging functionality for cancer applications," Soft Matter **7**(3), 839–856 (2011).
2. V. Torchilin, "Tumor delivery of macromolecular drugs based on the EPR effect," Adv. Drug Deliv. Rev. **63**(3), 131–135 (2011).
3. C. Oberle, U. Massing, and H. F. Krug, "On the mechanism of alkylphosphocholine (APC)-induced apoptosis in tumour cells," Biol. Chem. **386**(3), 237–245 (2005).
4. T. Koklič, R. Zeisig, and M. Šentjurc, "Interaction of alkylphospholipid liposomes with MT-3 breast-cancer cells depends critically on cholesterol concentration," Biochim. Biophys. Acta **1778**(12), 2682–2689 (2008).
5. J.-A. Conchello and J. W. Lichtman, "Optical sectioning microscopy," Nat. Methods **2**(12), 920–931 (2005).
6. T. Zimmermann, J. Rietdorf, and R. Pepperkok, "Spectral imaging and its applications in live cell microscopy," FEBS Lett. **546**(1), 87–92 (2003).
7. M. Eisenstein, "Something to see," Nature **443**(7114), 1017–1021 (2006).
8. M. Baker, "Laser tricks without labels," Nat. Methods **7**(4), 261–266 (2010).
9. M. Hintersteiner and M. Auer, "Single-bead, single-molecule, single-cell fluorescence: technologies for drug screening and target validation," Ann. N. Y. Acad. Sci. **1130**(1), 1–11 (2008).
10. I.-H. Kim, A. Järve, M. Hirsch, R. Fischer, M. F. Trendelenburg, U. Massing, K. Rohr, and M. Helm, "FRET imaging of cells transfected with siRNA/liposome complexes," Methods Mol. Biol. **606**, 439–455 (2010).
11. G. Zacharakis, R. Favicchio, M. Simantiraki, and J. Ripoll, "Spectroscopic detection improves multi-color quantification in fluorescence tomography," Biomed. Opt. Express **2**(3), 431–439 (2011).
12. R. Gräf, J. Rietdorf, and T. Zimmermann, "Live cell spinning disk microscopy," Adv. Biochem. Eng. Biotechnol. **95**, 57–75 (2005).
13. D. Toomre and J. B. Pawley, "Disk-scanning confocal microscopy," in *Handbook of Biological Confocal Microscopy*, J. B. Pawley, ed. (Springer, New York, 2006).
14. S. Pajk, M. Garvas, J. Štrancar, and S. Pečar, "Nitroxide-fluorophore double probes: a potential tool for studying membrane heterogeneity by ESR and fluorescence," Org. Biomol. Chem. **9**(11), 4150–4159 (2011).
15. R. Lansford, G. Bearman, and S. E. Fraser, "Resolution of multiple green fluorescent protein color variants and dyes using two-photon microscopy and imaging spectroscopy," J. Biomed. Opt. **6**(3), 311–318 (2001).

#146260 - $15.00 USD Received 21 Apr 2011; revised 3 Jun 2011; accepted 27 Jun 2011; published 29 Jun 2011

16. H. R. Morris, C. C. Hoyt, and P. J. Treado, "Imaging spectrometers for fluorescence and Raman microscopy: Acousto-optic and liquid crystal tunable filters," Appl. Spectrosc. **48**(7), 857–866 (1994).
17. Y. Hiraoka, T. Shimi, and T. Haraguchi, "Multispectral imaging fluorescence microscopy for living cells," Cell Struct. Funct. **27**(5), 367–374 (2002).
18. Y. Garini, I. T. Young, and G. McNamara, "Spectral imaging: principles and applications," Cytometry A **69A**(8), 735–747 (2006).
19. R. M. Zucker, P. Rigby, I. Clements, W. Salmon, and M. Chua, "Reliability of confocal microscopy spectral imaging systems: use of multispectral beads," Cytometry A **71A**(3), 174–189 (2007).
20. R. Zeisig, D. Arndt, R. Stahn, and I. Fichtner, "Physical properties and pharmacological activity *in vitro* and *in vivo* of optimised liposomes prepared from a new cancerostatic alkylphospholipid," Biochim. Biophys. Acta **1414**(1-2), 238–248 (1998).
21. R. M. Levenson and J. R. Mansfield, "Multispectral imaging in biology and medicine: slices of life," Cytometry A **69A**(8), 748–758 (2006).
22. S. J. Woltman, G. D. Jay, and G. P. Crawford, "Liquid-crystal materials find a new order in biomedical applications," Nat. Mater. **6**(12), 929–938 (2007).
23. M. E. Dickinson, G. Bearman, S. Tille, R. Lansford, and S. E. Fraser, "Multi-spectral imaging and linear unmixing add a whole new dimension to laser scanning fluorescence microscopy," Biotechniques **31**(6), 1272–1278, 1274–1276, 1278 (2001).
24. J. M. Lerner, N. Gat, and E. Wachman, "Approaches to spectral imaging hardware," Curr. Protoc. Cytom. **53**, 12.20.1–12.20.40 (2010).
25. T. Schmidt, G. J. Schütz, W. Baumgartner, H. J. Gruber, and H. Schindler, "Imaging of single molecule diffusion," Proc. Natl. Acad. Sci. U.S.A. **93**(7), 2926–2929 (1996).
26. R. F. M. de Almeida, J. W. Borst, A. Fedorov, M. Prieto, and A. J. W. G. Visser, "Complexity of lipid domains and rafts in giant unilamellar vesicles revealed by combining imaging and microscopic and macroscopic time-resolved fluorescence," Biophys. J. **93**(2), 539–553 (2007).
27. A. Esposito, A. N. Bader, S. C. Schlachter, D. J. van den Heuvel, G. S. Schierle, A. R. Venkitaraman, C. F. Kaminski, and H. C. Gerritsen, "Design and application of a confocal microscope for spectrally resolved anisotropy imaging," Opt. Express **19**(3), 2546–2555 (2011).
28. T. Zimmermann, "Spectral imaging and linear unmixing in light microscopy," Adv. Biochem. Eng. Biotechnol. **95**, 245–265 (2005).
29. A. Orthmann, R. Zeisig, T. Koklič, M. Šentjurc, B. Wiesner, M. Lemm, and I. Fichtner, "Impact of membrane properties on uptake and transcytosis of colloidal nanocarriers across an epithelial cell barrier model," J. Pharm. Sci. **99**(5), 2423–2433 (2010).
30. A. P. Demchenko, Y. Mély, G. Duportail, and A. S. Klymchenko, "Monitoring biophysical properties of lipid membranes by environment-sensitive fluorescent probes," Biophys. J. **96**(9), 3461–3470 (2009).
31. D. A. Erilov, R. Bartucci, R. Guzzi, A. A. Shubin, A. G. Maryasov, D. Marsh, S. A. Dzuba, and L. Sportelli, "Water concentration profiles in membranes measured by ESEEM of spin-labeled lipids," J. Phys. Chem. B **109**(24), 12003–12013 (2005).
32. H. M. Kim, H.-J. Choo, S.-Y. Jung, Y.-G. Ko, W.-H. Park, S.-J. Jeon, C. H. Kim, T. Joo, and B. R. Cho, "A two-photon fluorescent probe for lipid raft imaging: C-laurdan," ChemBioChem **8**(5), 553–559 (2007).
33. L. A. Bagatolli and E. Gratton, "A correlation between lipid domain shape and binary phospholipid mixture composition in free standing bilayers: A two-photon fluorescence microscopy study," Biophys. J. **79**(1), 434–447 (2000).
34. E. Munnier, S. Cohen-Jonathan, K. Herve, C. Linassier, M. Souce, P. Dubois, and I. Chourpa, "Doxorubicin delivered to MCF-7 cancer cells by superparamagnetic iron oxide nanoparticles: effects on subcellular distribution and cytotoxicity," J. Nanopart. Res. **13**(3), 959–971 (2011).

1. Introduction

Nanoparticles have reduced renal clearance and therefore remain in the blood circulation longer compared to compounds with lower molecular weight. Due to compromised vascular endothelial lining and the lack of lymphatic drainage they accumulate in the tumor environment [1]. Consequently, different nanoparticles, for example polymer-based, lipid-based, metal-based, and carbon-based nanoparticles, are increasingly being employed in cancer therapy [1]. The described enhanced permeability and retention effect can be exploited for passive targeting of high molecular weight compounds and small particles to tumors, which is currently considered as an effective way to bring drugs to tumors [2]. However, the efficient interaction of nanoparticles with cancer cells, e.g. through drug release in case of nanocarriers or through cellular uptake of nanoparticles, is as crucial as their accumulation around cells. Thus, it is important to develop advanced approaches to study mechanisms of nanoparticles delivery into cells.

In our previous work we have shown that the interaction of nanosized liposomes, made of cancerostatic alkylphospholipid [3] and cholesterol, with breast cancer cells depends critically on liposome membrane composition and membrane fluidity characteristics [4]. Although a

#146260 - $15.00 USD Received 21 Apr 2011; revised 3 Jun 2011; accepted 27 Jun 2011; published 29 Jun 2011

comprehensive membrane characterization based on electron paramagnetic resonance spectroscopy with spin labeling provided detailed information about overall membrane properties, it could not give spatial information about liposome-cell interaction. To gain new insight confocal fluorescence microscopy was used, since it enables localization of fluorescently labeled lipid nanoparticles.

Confocal fluorescence microscopy has become invaluable for a wide range of investigations due to its capability of imaging thin optical sections [5]. It is a convenient tool for localization of labeled regions within a sample, but it offers only limited information on their molecular properties. In addition, it does not allow differentiating between regions labeled with fluorescent probes with substantially overlapping spectra or sampling multiple spectral parameters simultaneously to understand the interactions of individual components within complex matrices. To overcome the shortcomings of confocal fluorescence microscopy spectral imaging or fluorescence microspectroscopy (FMS) has been introduced [6,7]. It has to be noted that there exist also label-free microscopy and microspectroscopy alternatives such as Raman microspectroscopy [8]. The label-free techniques are advantageous when the introduction of fluorescent labels and their instability pose a problem.

Confocal FMS indicates coupling of confocal fluorescence microscopy and spectroscopy. It allows acquisition of fluorescence spectra from particular volume elements in a sample. This technique has already proved to be a biomedically relevant methodology e.g. in drug screening [9], in studying cell transfection by liposomal formulation of siRNA [10], or in fluorescence tomography [11]. In the present work it will be shown that FMS methodology can be successfully applied also to the study of the mechanism of nanoparticles delivery into living cancer cells providing invaluable information that cannot be obtained with other methods.

In order to make FMS widely accessible to the biomedical community the system has to be affordable and should permit routine use. Here we report about such development of an FMS system based on a white light spinning disk confocal microscope. The spinning disk confocal microscopy is appropriate for cell imaging due to reduced fluorophore photobleaching problem as well as for a high image acquisition rate [12,13]. Moreover, the use of a broad-spectrum arc-lamp excitation (white light) source enables flexibility needed with respect to different problem-specific fluorescent probes as well as their synthesis-on-demand [14]. The white light FMS system is also in line with the current developments and ambitions focused to new fluorophore design with less limitation in the choice of excitation or emission wavelengths.

The developed FMS setup is an example of a filter-based system. Specifically, the emission wavelength selection is done with a narrow band liquid crystal tunable filter (LCTF) placed in front of the camera. A similar approach was used before [15], where however the LCTF was applied to resolve the weights of spectral components of different probes via linear unmixing and not for the detection of small lineshape changes in combination with environmentally sensitive probes. In similar manner to LCTF also acousto-optic tunable filters can be used [16]. Both filter technologies provide very fast wavelength selection and tunability while preserving image integrity with the advantage of having no moving parts. Beside the filter-based FMS systems, there are also interferometric, grating-based or optical-fiber-array-based systems [17,18].

The main advantage of our FMS system is its modular structure, which enables upgrade of any fluorescence microscope to a confocal FMS system at a relatively low cost and with a good spectral resolution. Since the system is flexible it can easily be optimized for different research problems.

In this paper we examine the mechanism of delivery of different fluorescently labeled nanoparticles into cancer cells by spectrally contrasting FMS images. The spectral information is obtained through automated analysis in terms of intensities and emission spectra maximum wavelengths from every pixel in FMS images. The application of a narrow band pass filter, i.e. LCTF, enabled us to localize and differentiate labeled nanoparticles and cell membranes although their spectra overlap. Moreover, the interaction of fluorescently

#146260 - $15.00 USD Received 21 Apr 2011; revised 3 Jun 2011; accepted 27 Jun 2011; published 29 Jun 2011

labeled nanoparticles with non-labeled cells has been also revealed through the influence of probes' local molecular environment on the spectral shape. The presented results point to the biomedical potential of the presented FMS setup.

2. Materials and methods

2.1. Test fluorescent beads

FocalCheck fluorescent beads (F36913, Invitrogen, Carlsbad, CA, USA) were chosen as a test sample. The convenience of this sample as a stable and repeatable standard has been demonstrated recently [19]. The test slide with immobilized fluorescent beads (6 μm in diameter) stained with two spectrally closely overlapping orange dyes was used. The excitation/emission maxima declared by the producer for these dyes are 541/555 and 545/565 nm, respectively. The FMS images were taken in 2 nm steps in the interval from 536 to 630 nm, exposure time being 500 ms for each of them. The maximum level of counts on the CCD detector was around 340 counts/s.

2.2. Interaction of cancer cells with fluorescently labeled nanoparticles

Human breast adenocarcinoma cell line MCF-7 cells were cultured in Dulbecco's modified Eagle's medium (DMEM, Gibco, Invitrogen, Carlsbad, CA, USA) containing 10% fetal calf serum (FSC) and 100 U/ml penicillin and 100 μg/ml streptomycin (Sigma-Aldrich Chemie GmbH, Steinheim, Germany). The cells were incubated at 37°C in a humidified 5% CO_2 atmosphere.

For fluorescence microspectroscopy experiments on the interaction of living cancer cells with different nanoparticles, cells were plated on glass-bottom cell culture dishes (Chambered Coverglass, Lab-Tek, Nalge Nunc, Rochester, NY) and allowed to grow for one day. The number of cells was approximately 30000 cells/well before the experiments.

In the experiments with fluorescein labeled polystyrene latex nanoparticles (Fluoresbrite YG microspheres, Polysciences GmbH, Eppelheim, Germany) of 50 nm diameter, 5 μl of 3.7×10^{12} particles/ml were incubated with cells for 20 minutes. For polymer nanoparticles with 500 nm diameter, 0.1 μl of 3.7×10^{11} particles/ml was used. These nanoparticles have the fluorescence emission maximum at 486 nm and an additional shoulder with intensity comparable to the maximum at around 515 nm, as declared by the producer. In our experiments the latter shoulder was monitored.

Afterwards 1 μl of 10^{-4} M or 5 μl of 10^{-3} M (dissolved in DMSO) lipophilic fluorescent probe NBD-FA was added to the cells in case of 50 nm or 500 nm nanoparticles, respectively. The different amount of lipophilic probe was used in order to approximately match the level of fluorescence emission by polymer nanoparticles in different cases. This precaution enabled contrasting between the label bound to the nanoparticles and the label in the cell membrane. Consequently, the exposure time of 500 ms for one optical slice at a single wavelength for 500 nm nanoparticles was increased to 20 s in the case of 50 nm nanoparticles when recording images in confocal mode. The maximum level of counts on the CCD detector in the regions free from aggregated nanoparticles was around 30 counts/s and 3 counts/s, respectively. The exposure time was 1 s for 50 nm nanoparticles in the wide-field mode with the maximum level of counts around 50 counts/s. The FMS images were taken in 3 nm steps in the interval from 470 to 551 nm.

NBD-FA probe was synthesized, as described earlier [14], by combining an amino sugar, which serves as a central polar group, NBD and the derivative of the fatty acid. The probe is labeled "16b" in the reference [14]. The measured emission maximum of this probe in a lipid environment was about 537 nm. Next, the time evolution of samples was followed with FMS.

In the experiments with lipid nanoparticles the cell medium was replaced with 200 μl PBS and then 10 μl of prepared labeled liposomes were added and incubated with the cultured cells. Next, the time evolution of samples was followed with FMS. The exposure time was 500 ms for single wavelength. The maximum level of counts on the CCD detector was around 260 counts/s for lipid nanoparticles with lower concentration of cholesterol and 80 counts/s

#146260 - $15.00 USD Received 21 Apr 2011; revised 3 Jun 2011; accepted 27 Jun 2011; published 29 Jun 2011

for nanoparticles with higher level of cholesterol. Due to considerable photobleaching of NBD-PC probe the FMS images were taken in 5 nm steps, so that fewer exposures were needed to obtain the whole spectrum. The spectral range was from 515 to 585 nm.

2.3. Preparation of fluorescently labeled liposomes

Large unilamellar vesicles (LUV) were prepared from octadecyl-(N,N-dimethyl-piperidino-4-yl)-phosphate (OPP), cholesterol (Chol) and dicetylphosphate (DCP), as described previously [20]. Briefly, multilamellar vesicles (MLV), final concentration 10 mM, were prepared by the lipid film/hydration method from appropriate mixtures of stock solutions of the components in CH_3Cl/MeOH (7:3, v/v). The lipid film was resuspended in phosphate buffer saline (PBS). LUV were prepared from MLV by repeated extrusion through polycarbonate filters (diameter of pores, 100 nm) using a LiposoFast Basic system (Avestin, Ottawa, ON, Canada). The molar ratio between OPP and DCP was kept constant (10:2), while the molar ratio between OPP and Chol was different for different liposomes. In OPP5 LUV the molar ratio of OPP:Chol was 10:5 and in OPP15 the molar ratio was 10:15. The negatively charged DCP was used to prevent aggregation of LUV.

LUV were fluorescently labeled with a phospholipid fluorescent probe NBD-PC, where 7-nitrobenz-2-oxa-1,3-diazol-4-yl (NBD) is attached to a phosphatidylcholine phospholipid (16:0-06:0 NBD PC, Avanti polar lipids, Alabaster, AL, USA). NBD-PC was added to the organic solvent before preparing MLV. The fluorescence emission maximum of this probe declared by the producer is around 534 nm. The molar concentration of the fluorescent probe with respect to other components was 0.5 mol%.

The reference measurements of fluorescence emission spectra were done with Infinite M1000 microplate reader (Tecan, Männendorf, Switzerland). A 96-well black plate was used in the fluorescence intensity top mode.

2.4. Confocal fluorescence microspectroscopy system

The confocal FMS system, presented in Fig. 1, is built on an inverted microscope Nikon Eclipse TE 2000-E platform. Unless specified otherwise, an oil immersion 100x 1.4-NA objective lens was used in this work to provide high magnification and high spatial resolution. The microscope is equipped with a Prior ProScan II (Cambridge, UK) motorized and computer controlled stage that enables precise movements of the sample in the x and y directions (in the plane perpendicular to the optical axis of the objective). Focus is controlled with a stepper motor for objective holders, which enables optical sectioning along the z direction (along the optical axis). The confocal unit is a CARV II spinning disk confocal module (BD Biosciences, Franklin Lakes, NJ, USA), which also houses excitation, dichroic and emission filters (BrightLine filters from Semrock, Rochester, NY, USA). As an excitation source a high power 300 W xenon Lambda LS arc-lamp (Sutter, Novato, CA, USA) is used. The advantage of this kind of source is a broad spectrum of emitted light, which provides flexibility with respect to the wavelength of excitation light. All electronic microscope functions as well as camera control, shutters, stage, and focus, are controlled using a home-built software.

The fluorescence emission light that leaves the CARV unit can be directed to the camera in two ways. In the microspectroscopy mode the light goes through the liquid crystal tunable filter (LTCF) [21,22] (Fig. 1a). In the other alternative, the light goes directly to the camera by inserting the movable mirrors for conventional microscopy operation (Fig. 1b). The lenses in the latter option are used to correct for the focus shift produced by passing light through the LCTF. In our case the geometrical constraints and the degree of the focus shift due to LCTF prompted us to use in turn achromatic convergent lens with the focal length of 10 cm and an achromatic divergent lens with the focal length of 5 cm. The magnification of this double lens combination is approximately 1.5, which is matched on the first path by using the 1.5x magnification optovar in the Nikon microscope.

#146260 - $15.00 USD Received 21 Apr 2011; revised 3 Jun 2011; accepted 27 Jun 2011; published 29 Jun 2011

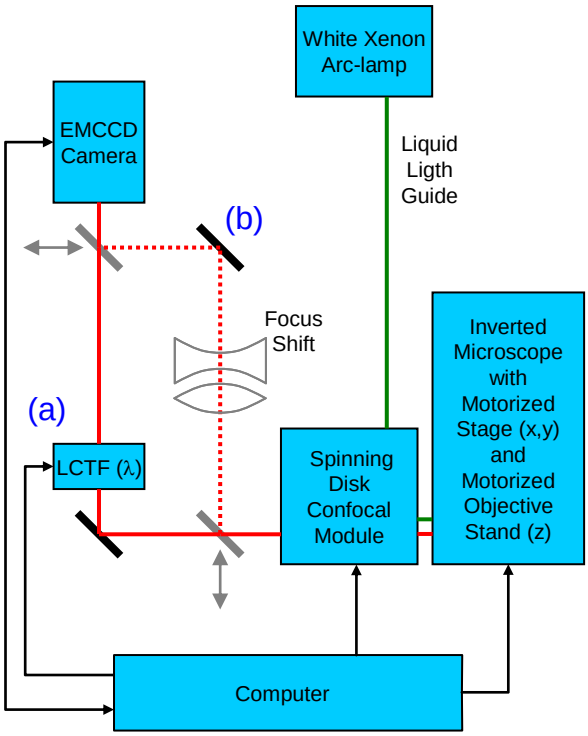

Fig. 1. A schematic presentation of the configuration of the experimental setup. The light coming from the spinning disk confocal module can be directed to the camera in two different paths by moving two mirrors (indicated by the double-headed arrows) in or out of the optical path. The first path (a) where the light goes through the LCTF represents the (confocal) fluorescence microspectroscopic mode while the second path (b) represents the conventional (confocal) fluorescence microscopy imaging mode.

The microspectroscopic images are taken successively at different wavelengths, i.e. as a wavelength stack or λ-stack. The LCTF is Varispec VIS-10-20 from CRi (Woburn, MA, USA), tunable in the range from 400 to 720 nm, with the bandwidth of around 10 nm. The uncertainty in setting the wavelength value of LCTF is about 1 nm. Both the wavelength accuracy and the LCTF bandwidth are well below the fluorescence emission spectral width, thus exhibiting very low distortion on the acquired emission spectra. The wavelength can be changed in the order of a few tens of milliseconds.

The last component in the system is a highly sensitive QImaging Rolera MGi back-illuminated EMCCD (Electron Multiplying Charge-Coupled Device) (Surrey, BC, Canada) camera with a very high quantum efficiency (>90% between 500 and 700 nm), which is needed mainly because of the light intensity losses due to spinning disk and LCTF. The detector has 512x512 pixels with 16 μm pixel size. The image size on the detector matches the part of homogeneously illuminated section of the sample. The detector field of view determines the size of a single image pixel to about 100 nm x 100 nm, which does not exceed half of the wavelength. The EM assures adequate signal to noise ratios also at fast image acquisition rate enabled by the spinning disk confocal microscope.

The measured radiant output from the liquid light guide connected to the xenon lamp is around 450 mW being reduced to around 25 mW when light reaches the sample. In confocal mode spinning disk reduces the value by additional 92% (measured value), yielding approximately 2 mW of excitation power or 10^{16} photons/s. Assuming the number of dye molecules in a volume element of a sample to be around 1000 (corresponding to 10^{-5} M probe solution or 1 probe per 200 lipid molecules in a vertical membrane bilayer) and taking into account typical extinction coefficient and quantum efficiency (2×10^4 (M cm)$^{-1}$, and 0.3,

#146260 - $15.00 USD Received 21 Apr 2011; revised 3 Jun 2011; accepted 27 Jun 2011; published 29 Jun 2011

respectively), their fluorescent output is around 2.0×10^6 and 1.5×10^5 photons/s in wide-field and confocal mode, respectively. Considering objective acceptance angle, dichroic and emission filter transmittances, LCTF characteristics, and camera quantum efficiency, around 8000 or 600 photons/s are finally detected within 10 nm LCTF-filtering window in wide-field or confocal mode, respectively. Consequently, the number of counts on the CCD detector will be in the range of hundred counts/s or ten counts/s after AD conversion in wide-field or confocal mode, respectively. This can be increased mainly by more efficient probe or increased probe concentration.

In our system the typical spectral acquisition time for single optical slice is in the range of minutes. In comparison, typical acquisition times in wavelength dispersive systems for 512x512 pixels image range from seconds to tens of minutes [23,24]. The main advantage of an LCTF-based system over systems with simultaneous channels relies on the spectral resolution at desired sensitivity. The latter system working in a broad spectral range (e.g. 32 channels and 300 nm spectral range) provides resolution of 10 nm at a channel width of 10 nm. With respect to a typical fluorescence spectrum span of about 80 nm, such a device provides only 8 points characterizing the emission spectrum. An LCTF-based system can be adjusted to 1 nm steps with 10 nm filter width, providing better resolution at a comparable sensitivity. Note, that the distortion of a lineshape is still small since the linewidth is much larger than 10 nm. On the contrary, when working in a narrow spectral range, like 30-60 nm, a 32 channel system would have the same resolution but with 1 nm channel width. Consequently, the exposure times would have to be increased for 10 times to count the same amount of photons. Similar conclusions hold for wavelength dispersive systems based on CCD camera, where binning increases sensitivity at a cost of lower spectral resolution. Taking these facts into account, we can state that our FMS system can perform better for a full-image high-resolution microspectroscopic analysis, while the point-scanning wavelength dispersive systems are advantageous in cases when just a portion of the image has to be scanned.

2.5. Spectra acquisition and analysis

A home-built program "FMS+: Fluorescence MicroSpectroscopy Acquisition, Control, Processing" has been developed in MathWorks MatLab environment (Natick, MA, USA). The program controls the recording of images at different wavelengths and their analysis in order to extract fluorescence emission spectra. The program replaces the software packages controlling the microscope, camera and LCTF and, most importantly, allows high-throughput microspectroscopy experiments. The latter is not possible by independent control over the different components of the FMS system.

To obtain spectra that can be directly compared to spectroscopic data acquired by other methods, several corrections have to be applied to the pixel intensity values measured by the detector. The camera dark current is corrected by acquiring two black reference images before and after the experiment with the same camera settings but without excitation light. An average of these images is subtracted from all images in a spectral series.

Photobleaching of the fluorophores is corrected with a similar approach by monitoring the intensity of the signal recorded at a reference wavelength that can be arbitrarily chosen (usually close to the wavelength of maximal intensity in the considered spectral region). During the recording of a λ-stack six reference images are taken (one at the beginning, four during the recording at recurring wavelength intervals, and one at the end), and the decay of the intensity over the consecutive reference images is used to correct the intensities of each image in the λ-stack after the dark current contribution has been subtracted.

Transmission characteristics of the LCTF as well as the EMCCD sensitivity as a function of wavelength are known and are utilized to correct the light intensities at each wavelength accordingly [15]. Since transmittances of fluorescence filters used are high (> 0.95) and nearly constant (with variations < ± 2%, which occur at much smaller wavelength steps than LCTF spectral width) in the spectral region of typical measurements, their effect on the measured spectra is neglected.

#146260 - $15.00 USD Received 21 Apr 2011; revised 3 Jun 2011; accepted 27 Jun 2011; published 29 Jun 2011

After the images in a λ-stack are corrected, as described above, a spectrally contrasted image is generated for a fast and intuitive visual inspection of the acquired data from the obtained spectra. Every point of the image is color-coded in terms of hue $h \in [0,1]$ according to the wavelength of the spectral maximum λ_{max}, and in terms of brightness $v \in [0,1]$ according to the level of intensity $i \in [0,1]$. The latter is normalized to the maximum intensity in the λ-stack of images, respectively. The pixel colors are defined according to the following formulae:

$$h = 0.8\left(1 - \left(\frac{\lambda_{max} - \lambda_1}{\lambda_2 - \lambda_1}\right)^{1.2}\right)^{1.3}, \quad s = 1, v = i^{0.5}, \tag{1}$$

where λ_1 and λ_2 are predefined values limiting the wavelength range of interest. Saturation is always kept maximal (equal to 1) for best color contrast. Values of λ_{max} that fall outside this range are set to the limiting values. The exponents in Eq. (1) are introduced to enhance the perception of color contrast while the coefficient of 0.8 extracts violet-to-red color range from cyclic hue function.

In case of low signal-to-noise ratio and small differences in the fluorescence emission spectrum maxima, the noise in the detected photon counts can interfere with the measurement of very small shifts. To reduce the effect of noise on the determination of λ_{max} position spectral data is smoothed by fitting it with a third order polynomial. Subsequently, a normalized distribution of λ_{max} values can be plotted for an arbitrarily chosen image region and the maximum of the histogram is then used as the reference emission spectrum maximum λ_{max}(hist). As it can be seen from the experimental data, such a procedure reveals λ_{max}(hist) accuracy better than 1 nm, even despite lower spectral resolution for spectra taken with wavelength steps of a few nm. Note that this procedure is analogous to the single molecule tracking, where optical resolution of 200 nm is converted to positional accuracy of 30 nm by fitting the shape of the light profile [25].

3. Results and discussion

3.1. Spectral contrasting of microspectroscopic image

By passing the emitted light through LCTF, FMS system is running in the fluorescence microspectroscopic mode (Fig. 1a). The FMS mode can either be confocal or wide-field depending on the positioning of the spinning disk in the optical path. The pictures taken at different wavelengths are used to build a λ-stack of images (Fig. 2a). An example in Fig. 2 shows an optical slice through two fluorescent beads. The two beads are labeled with two different fluorescent dyes with the declared emission maxima at 555 and 565 nm.

The "FMS+" software enables extraction of fluorescence emission spectra from any pixel in the image or an average spectrum from a group of neighboring pixels (small white squares in Fig. 2a). As shown in Fig. 2b, test example of two fluorescent beads reveals a measured shift between the maxima of fluorescence emission spectra of around 9 nm, which agrees well with the shift of around 10 nm declared by the producer of the beads.

The color coding transformation automatically assigns colors to pixels or groups of pixels across the image according to particular emission spectrum characteristics as discussed in the section Materials and methods. In the presented case the color coding was applied to code λ_{max} with the underlying color legend (small open white squares in Fig. 2b) within the interval from 540 to 570 nm. Consequently, the pixels corresponding to the left fluorescent bead will be colored bright green in the final image, while the right bead will be orange/red and dimmer, since the spectrum intensity is lower. In the spectrally contrasted image (Fig. 2c) small white squares indicate the positions that were originally chosen in the λ-stack (Fig. 2a) for presenting fluorescence emission spectra.

Note that in contrast to the LCTF application of Fraser's group [15], where LCTF is used to derive locally resolved spectral information of different probes linearly unmixed via known

#146260 - $15.00 USD Received 21 Apr 2011; revised 3 Jun 2011; accepted 27 Jun 2011; published 29 Jun 2011

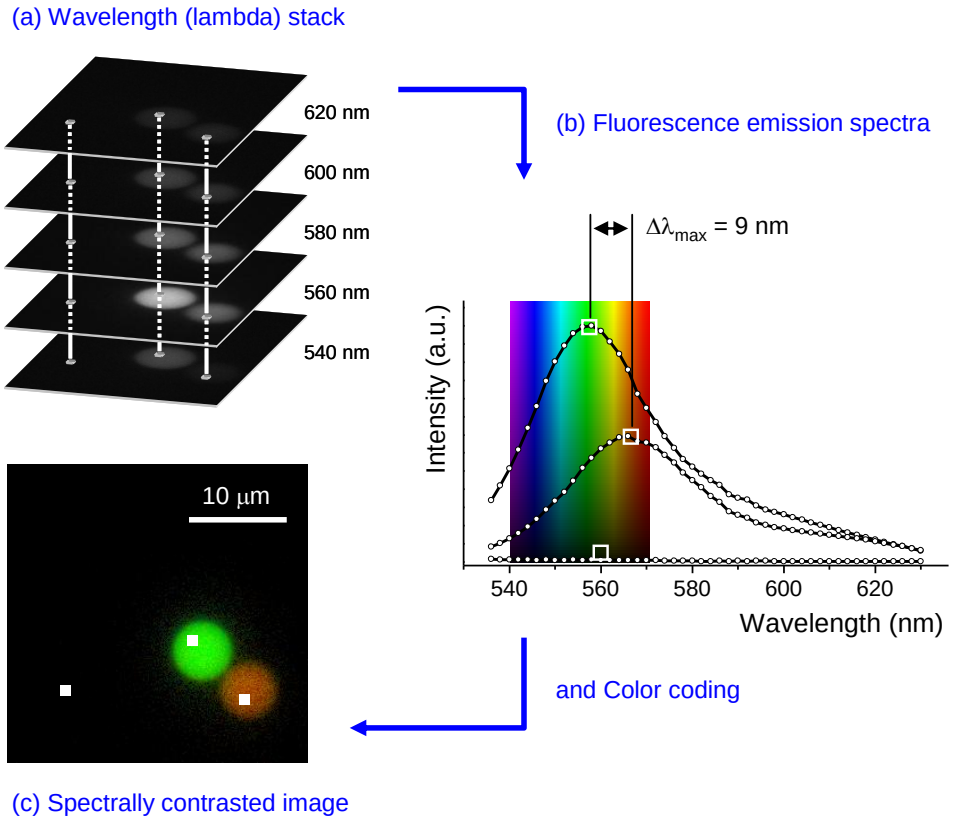

Fig. 2. Spectral contrasting of a microspectroscopic image. (a) Fluorescence microspectroscopic mode provides a stack of images obtained at different wavelength settings of the LCTF (a λ-stack of images) in FMS system. Different regions of interest can be selected from which (b) fluorescence emission spectra are extracted. The spectra are used in the color coding procedure to provide (c) a spectrally contrasted image, in this case the confocal image of equatorial optical slice through fluorescent beads. For details see text.

and predetermined spectral lineshapes, in our case spectral lineshapes are analyzed in terms of wavelengths of maximal intensities λ_{max}. While in the first case the derived weights are directly encoded by the RGB colors, in our case spectral maxima are transformed into colors using the hue rule characterizing changed local concentration or environment when using environmentally sensitive probes. The two approaches are therefore complementary – the first one enables spectral decomposition and concentration detection, while the latter enables the characterization of small changes in environment detected by one probe only.

The main benefit of the color coding is a fast recognition of spectral variations across the image. Similar spectral contrasting approaches have been utilized in other microspectroscopic techniques, for instance in fluorescence lifetime imaging microscopy (FLIM), where an image can be color-coded in a way to highlight the different fluorescence lifetimes in different parts of the sample [26]. Another example is spectrally resolved anisotropy imaging, where the degree of fluorescence anisotropy is used for the color coding [27].

3.2. Study of polymer nanoparticles delivery into cancer cells

Spatially-resolved spectral analysis, which is enabled through the FMS system, allowed us to track nanoparticles' delivery/uptake into cancer cells. Firstly, experiments with incubation of cells with polymer nanoparticles of two different diameters (50 and 500 nm) were performed. After the initial incubation with nanoparticles the lipophilic NBD-FA probe was added to

#146260 - $15.00 USD Received 21 Apr 2011; revised 3 Jun 2011; accepted 27 Jun 2011; published 29 Jun 2011

enable co-localization of nanoparticles with plasma membrane and cell inner membrane structures. In our case the emission spectra of fluorescent labels attached to nanoparticles and labels introduced in cell membranes overlap. Therefore, the use of FMS and spectral contrasting enables to identify and spatially distinguish the two labels.

In the intensity confocal images the interior of the cells fluoresces (Figs. 3a.1–3c.1), but it is not possible to determine the origin of this fluorescent light, i.e. whether it comes from nanoparticles or lipophilic probe, except for the aggregated nanoparticles. It can also be seen from comparison of images taken in the wide-field and confocal mode (Figs. 3a and 3b) that in the wide-field mode the regions rich in the membrane probe seem larger due to the out-of-focus light coming from the membranes above and below the focal plane.

On the contrary, the color-coded images in Figs. 3b.2 and 3c.2 clearly show the difference in behavior between nanoparticles of different size. It can be seen that only 50 nm nanoparticles were transferred in the interior of cells after 25 minutes of incubation (Fig. 3b.2), while the 500 nm nanoparticles, even after 2 hours, remained outside the cells (Fig. 3c.2). Co-localization was enabled through spectral identification despite substantial spectral overlap of the probes on the nanoparticles and in cell membranes (Fig. 3b.2). If quantitative information is desired about the overlapping probes, one should apply the method of linear unmixing [15,23,28].

3.3. Study of lipid nanoparticles delivery into cancer cells

Although confocal fluorescence microscopy was previously used to test OPP liposomes as drug nanocarriers [29], it did not reveal the mechanism of OPP liposomes delivery across plasma membrane. For optimization of the liposomes' properties for even larger cancerostatic efficiency, FMS was applied to study living cancer cells exposed to OPP lipid nanoparticles. OPP liposomes were labeled with the environment-sensitive NBD-PC fluorescent probe. Note that the cells were not labeled.

NBD is an example of a solvatochromic dye that can exhibit shifts in its emission spectra as a function of polarity and hydration of its environment [30]. Consequently, any fusion of the OPP liposomes with different amount of cholesterol relative to the cancer cell membrane should lead to a change in the lipid environment of the NBD-PC probe. This should induce a shift in the λ_{max} of the corresponding emission spectrum, since the level of cholesterol influences the polarity and hydration profile in the membrane [31]. The ability of the FMS of spatially-resolved spectral analysis was therefore used to trace the fusion of cancer cell membranes and OPP liposomes with different OPP/cholesterol ratios, referred to as OPP5 (29 mol% Chol) and OPP15 (56 mol% Chol).

First the environmental sensitivity of NBD-PC was examined in the case of pure liposome samples. The images were acquired with FMS and objective lens with 10x magnification. The spectra were obtained by averaging the signal from the whole image. The lower magnification and averaging was applied in order to reproduce experimental conditions in measurements with fluorimeter. The results showed that the spectrum of OPP15 LUV is shifted to lower wavelengths for about 5 nanometers compared to the spectrum of OPP5 LUV (data not shown). This result was confirmed also by reference measurements on fluorimeter.

The reference spectra of liposomes were acquired with FMS and objective lens with 100x magnification also on mixture of cells and liposomes. For this purpose, images were spectrally analyzed in the regions outside the cells, where intact liposomes that do not interact with cells are present. These regions are depicted by the open green square for OPP5 liposomes in Fig. 4a.4 and by the open dark blue square for OPP15 nanoparticles in Fig. 4b.4. Value of λ_{max}(hist) for intact OPP5 liposomes obtained from the histogram in Fig. 4 (green columns) is downshifted for about 3 nm with respect to intact OPP15 liposomes (dark blue columns). The shift qualitatively confirms the observations for pure liposome samples. The difference in the measured shifts arises from different experimental conditions. Especially, photobleaching, which is intensified when the lens with 100x magnification is used compared to the lens with 10x magnification, imposes additional uncertainty to the absolute value of λ_{max}.

#146260 - $15.00 USD Received 21 Apr 2011; revised 3 Jun 2011; accepted 27 Jun 2011; published 29 Jun 2011

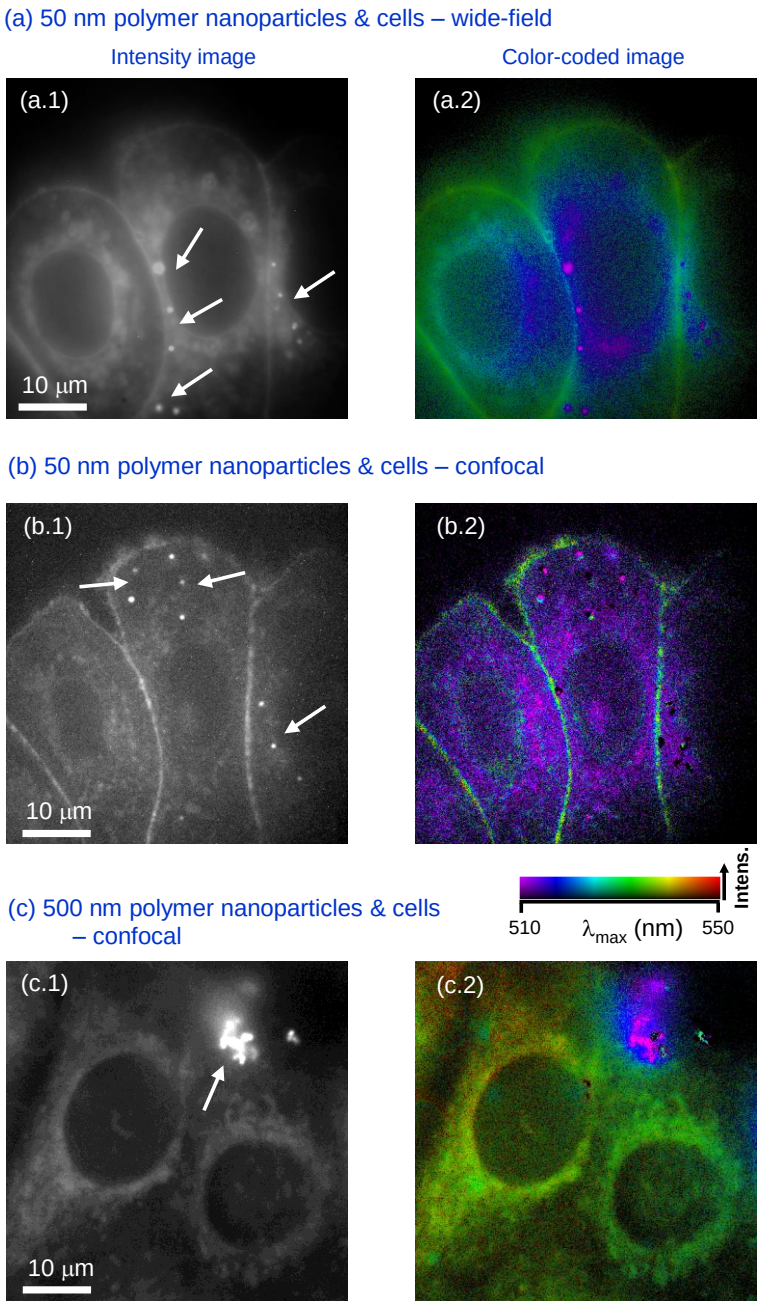

Fig. 3. Interaction of polystyrene nanoparticles with living MCF-7 human breast cancer cells. Images of cells incubated *in vitro* with NBD-FA probe, i.e. a lipophilic NBD based fluorescent probe, and with (a) fluorescent 50 nm polymer nanoparticles imaged in wide-field mode or (b) imaged in confocal mode and with (c) 500 nm nanoparticles imaged in confocal mode. (a.1, b.1, c.1) Fluorescence intensity contrasted images. Fluorescent emission spectra of the nanoparticles and the lipophilic probe overlap, so it is not possible to determine the delivery efficiency of nanoparticles to the cancer cells from microscopic image, except for the aggregated nanoparticles indicated by arrows. (a.2, b.2, c.2) Spectrally contrasted images, which show the distribution of the NBD-FA probe (green/yellow) and fluorescein (violet/blue). The observed colors correspond to the measured (537 nm) and declared (shoulder at 515 nm) emission maximum values for membrane and nanoparticle probe, respectively.

#146260 - $15.00 USD Received 21 Apr 2011; revised 3 Jun 2011; accepted 27 Jun 2011; published 29 Jun 2011

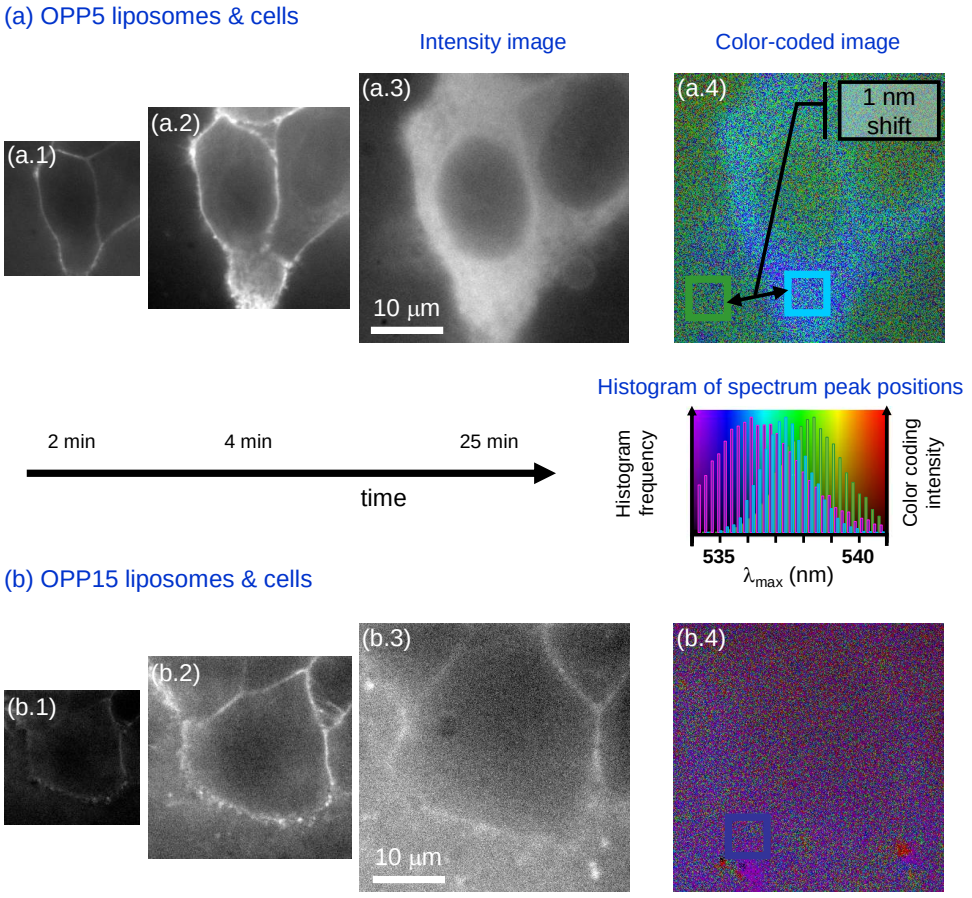

Fig. 4. Interaction of OPP lipid nanoparticles with living MCF-7 human breast cancer cells. Cells incubated *in vitro* with (a) 100 nm OPP5 LUV labeled with NBD-PC or with (b) labeled OPP15 LUV. (a.1-a.3, b.1-b.3) The time evolution of the intensity contrasted images of the cancer cells. (a.4, b.4) Color-coded images corresponding to the last image in the time line. Between the two color-coded images the histogram of the distribution of fitted spectrum peak positions (λ_{max}) from the accordingly-colored squared regions in a.4 and b.4 are shown. The histogram confirms the significance of the observed small shifts in the λ_{max}(hist) value.

The relatively small observed shift between spectra of OPP liposomes with different amount of cholesterol ascertains the need of a narrow band pass filter system, which would not be required for well separated spectra. In the latter case two different excitation/dichroic/emission filter combination can be used and subsequently the integrated fluorescence emission intensities can be compared for the two combinations. Such an approach is used in ratiometric or generalized polarization measurements [30,32,33].

To trace the interaction of the OPP liposomes with the living cancer cells, the time evolution of the delivery was followed. It seems that OPP5 gradually accumulate in the cells (compare Fig. 4a.1 to Fig. 4a.3). On the other hand, OPP15 did neither interact nor accumulate in cells (Fig. 4b.1 to Fig. 4b.3). This confirms that the efficiency of delivery depends on the amount of cholesterol in OPP liposomes, which is in agreement with our previous results obtained by electron paramagnetic resonance [4]. Lack of OPP15 liposomes accumulation in the cells means that these liposomes are spread and diluted all-around the cells, significantly increasing out-of-focus light and thus decreasing the contrast in confocal mode. Together with low intensity (low signal to noise ratio) this forced us to show the wide-field image for OPP15. To enable better comparison with OPP5 also the latter is shown in the wide-field mode, although we obtained also confocal FMS data.. For this particular

#146260 - $15.00 USD Received 21 Apr 2011; revised 3 Jun 2011; accepted 27 Jun 2011; published 29 Jun 2011

experiment this did not impose a limitation, while the spectral information was collected from a larger spatial region of the sample, as discussed below.

Finally, FMS reveals much more than just information on the accumulation of the particles within the cells. It is also possible to see a change in spectral properties of NBD-PC from the color-coded image of cancer cells exposed to OPP5 liposomes. Specifically, there is a spectral shift between the spectra of the probe residing inside the cell (Fig. 4a.4, area depicted by the open light blue square) or in intact free liposomes (Fig. 4a.4, area depicted by the open green square). The analysis of the distribution of fitted spectrum peak positions λ_{max}, shown in a histogram, clearly reveals the shift of 1 nm, which is significant although very small (compare the center of mass for green and light blue columns in the histogram in Fig. 4). Note that the increased accuracy of determining spectral maximum position is analogous to an increased positional accuracy in single molecule tracking (see Section 2.5 for details). Since the spectrum of NBD-PC depends on the properties of lipid environment as already corroborated above, it is possible to assign the spectral shift to a change in the probe environment. The main reason for this change is mainly due to direct interaction of liposomes with cell membrane, e.g. through membrane fusion. In contrast, the analysis of the OPP15 liposomes data shows no significant difference in the spectral properties across the image (Fig. 4b.4). Due to the wide-field mode, which imposes a large portion of out-of-focus light, we can see the same (weak) spectrum all over the image.

The presented example clearly shows the strength of the FMS approach in the study of the mechanism of nanoparticles interaction with cancer cells. Similarly to lipid-based nanoparticles, the usefulness of the FMS approach to study drug delivery to cancer cells was also shown for metal-based nanoparticles [34].

4. Conclusions

Different nanoparticles are increasingly being used in cancer therapy because of their passive targeting to cancer cells by enhanced permeability and retention effect. The results presented in the current work show that the developed modular fluorescence microspectroscopy system can serve as a useful biomedical tool to study and screen the mechanisms of delivery of different fluorescently labeled nanoparticles to living cancer cells. Firstly, FMS enables co-localization of inner cancer cell membranes and cell-entering polymer nanoparticles that are labeled with spectrally overlapping fluorophores. Secondly, FMS made it possible to detect a small shift in the fluorescence emission spectrum maximum, which was attributed to the fusion of labeled lipid nanoparticles with cancer cell membranes. In addition, the built system represents a diverse tool for research of fluorescently labeled biological systems, e.g. for monitoring biophysical properties of lipid membranes by environmentally sensitive fluorescent probes.

Acknowledgments

This work was carried out with financial support from Slovenian Research Agency (program No. P1-0060) and financial support in the framework of Center of Excellence NAMASTE. We would also like to thank Mr. Hugo Ostermann from Chromaphor and Dr. Andrea Latini from Crisel Instruments companies for useful advices concerning the CARV II confocal module. We would like to acknowledge the contribution of Dr. Iztok Dogša to the development of the FMS system. We are grateful to Dr. Stane Pajk and Prof. Slavko Pečar from the University of Ljubljana, Faculty of Pharmacy, for synthesizing the fatty-acid-NBD-based fluorescent probe and to Prof. Igor Križaj from Jožef Stefan Institute for providing access to the Tecan microplate reader.

#146260 - $15.00 USD Received 21 Apr 2011; revised 3 Jun 2011; accepted 27 Jun 2011; published 29 Jun 2011